Report

Current Biology

Distinct Roles of RZZ and Bub1-KNL1 in Mitotic Checkpoint Signaling and Kinetochore Expansion

Highlights

- RZZ mediates a temporal switch in how Mad1-Mad2 is recruited to kinetochores
- Mps1 phosphorylates Rod's N terminus to trigger fibrous corona formation
- Mad1-Mad2 requires a non-receptor activity of Bub1 to inhibit anaphase
- Nonsense-associated alternative splicing can circumvent *BUB1* disruption

Authors

Jose-Antonio Rodriguez-Rodriguez, Clare Lewis, Kara L. McKinley, ..., Alexey Khodjakov, Iain M. Cheeseman, Prasad V. Jallepalli

Correspondence

jallepap@mskcc.org

In Brief

Rodriguez-Rodriguez et al. identify distinct roles for Bub1, KNL1, and RZZ in SAC signaling and fibrous corona formation. They also show that BUB1-disrupted clones re-express Bub1 and regain SAC function via nonsense-associated alternative splicing, an often-overlooked transcriptional response that can limit penetrance in genome editing experiments

Rodriguez-Rodriguez et al., 2018, Current Biology *28*, 1–8
November 5, 2018
https://doi.org/10.1016/j.cub.2018.10.006

CellPress

Please cite this article in press as: Rodriguez-Rodriguez et al., Distinct Roles of RZZ and Bub1-KNL1 in Mitotic Checkpoint Signaling and Kinetochore Expansion, Current Biology (2018), https://doi.org/10.1016/j.cub.2018.10.006

Current Biology
Report

Distinct Roles of RZZ and Bub1-KNL1 in Mitotic Checkpoint Signaling and Kinetochore Expansion

Jose-Antonio Rodriguez-Rodriguez,[1] Clare Lewis,[1] Kara L. McKinley,[2,3] Vitali Sikirzhytski,[4,5] Jennifer Corona,[1] John Maciejowski,[1] Alexey Khodjakov,[4,5] Iain M. Cheeseman,[2,3] and Prasad V. Jallepalli[1,6,*]
[1]Molecular Biology Program, Sloan Kettering Institute, Memorial Sloan Kettering Cancer Center, New York, NY, 10065, USA
[2]Whitehead Institute for Biomedical Research, 9 Cambridge Center, Cambridge, MA 02142, USA
[3]Department of Biology, Massachusetts Institute of Technology, Cambridge, MA 02142, USA
[4]Wadsworth Center, New York State Department of Health, Albany, NY 12201, USA
[5]Rensselaer Polytechnic Institute, Troy, NY 12180, USA
[6]Lead Contact
*Correspondence: jallepap@mskcc.org
https://doi.org/10.1016/j.cub.2018.10.006

SUMMARY

The Mad1-Mad2 heterodimer is the catalytic hub of the spindle assembly checkpoint (SAC), which controls M phase progression through a multi-subunit anaphase inhibitor, the mitotic checkpoint complex (MCC) [1, 2]. During interphase, Mad1-Mad2 generates MCC at nuclear pores [3]. After nuclear envelope breakdown (NEBD), kinetochore-associated Mad1-Mad2 catalyzes MCC assembly until all chromosomes achieve bipolar attachment [1, 2]. Mad1-Mad2 and other factors are also incorporated into the fibrous corona, a phospho-dependent expansion of the outer kinetochore that precedes microtubule attachment [4–6]. The factor(s) involved in targeting Mad1-Mad2 to kinetochores in higher eukaryotes remain controversial [7–12], and the specific phosphorylation event(s) that trigger corona formation remain elusive [5, 13]. We used genome editing to eliminate Bub1, KNL1, and the Rod-Zw10-Zwilch (RZZ) complex in human cells. We show that RZZ's sole role in SAC activation is to tether Mad1-Mad2 to kinetochores. Separately, Mps1 kinase triggers fibrous corona formation by phosphorylating two N-terminal sites on Rod. In contrast, Bub1 and KNL1 activate kinetochore-bound Mad1-Mad2 to produce a "wait anaphase" signal but are not required for corona formation. We also show that clonal lines isolated after *BUB1* disruption recover Bub1 expression and SAC function through nonsense-associated alternative splicing (NAS). Our study reveals a fundamental division of labor in the mammalian SAC and highlights a transcriptional response to nonsense mutations that can reduce or eliminate penetrance in genome editing experiments.

RESULTS

The RZZ Complex Is Required to Maintain SAC Arrest, but Not to Initiate It

To analyze RZZ's roles in fibrous corona assembly and SAC signaling, we used adeno-associated virus (AAV) and CRISPR/Cas9 to modify both alleles of *KNTC1* (Rod) in HCT116 cells, a diploid human colorectal cell line (Figures S1A–S1C). $KNTC1^{HF/-}$ (hypomorph-flox) cells expressed Rod at ~20% of the wild-type level (Figure S1D) and exited mitosis prematurely when microtubule polymerization (nocodazole, 99 ± 6 min SEM) or spindle bipolarity (S-trityl-L-cysteine [STLC], 193 ± 9 min) were inhibited. In contrast, wild-type cells never exited mitosis during the 16-hr time lapse (Figure 1A). We obtained viable $KNTC1^{-/-}$ clones after expressing Cre recombinase that were as SAC defective as $KNTC1^{HF/-}$ cells (Figures 1A and S1E). Early escape from spindle-poison-induced mitotic arrest was also observed in $KNTC1^{-/-}$ human retinal pigment epithelial (RPE) cells and *KNTC1*, *ZW10*, and *ZWILCH* KO HeLa cells (Figures 1B, 1C, and S1F–S1I). On the other hand, untreated RZZ-null cells had longer and more heterogenous mitotic timing, suggesting frequent but transient SAC activation (Figure 1D). Consistently, inhibition of the SAC kinase Mps1 caused $KNTC1^{-/-}$ cells to exit mitosis with wild-type kinetics (Figure 1D). These observations suggest that RZZ maintains (but does not initiate) SAC signaling at unattached or improperly attached kinetochores in multiple human cell types.

RZZ Mediates a Temporal Switch in How Mad1-Mad2 Is Targeted to Kinetochores

To understand RZZ's impact on mitotic chromosome and SAC signaling dynamics, we expressed and imaged H2B-mCherry and FLAG-GFP-TEV-S peptide (FLAP)-Mad1 using spinning disk confocal microscopy. Mad1 first localized at kinetochores at nuclear envelope breakdown (NEBD) and then dissociated as chromosomes congressed at the metaphase plate (Figure 1E and Video S1; n = 10 cells). Congression was less efficient in $KNTC1^{-/-}$ cells, consistent with the lack of Spindly and dynein at kinetochores [15] (Figures S1F–S1I), but Mad1 was still targeted to misaligned chromosomes as effectively as in wild-type cells

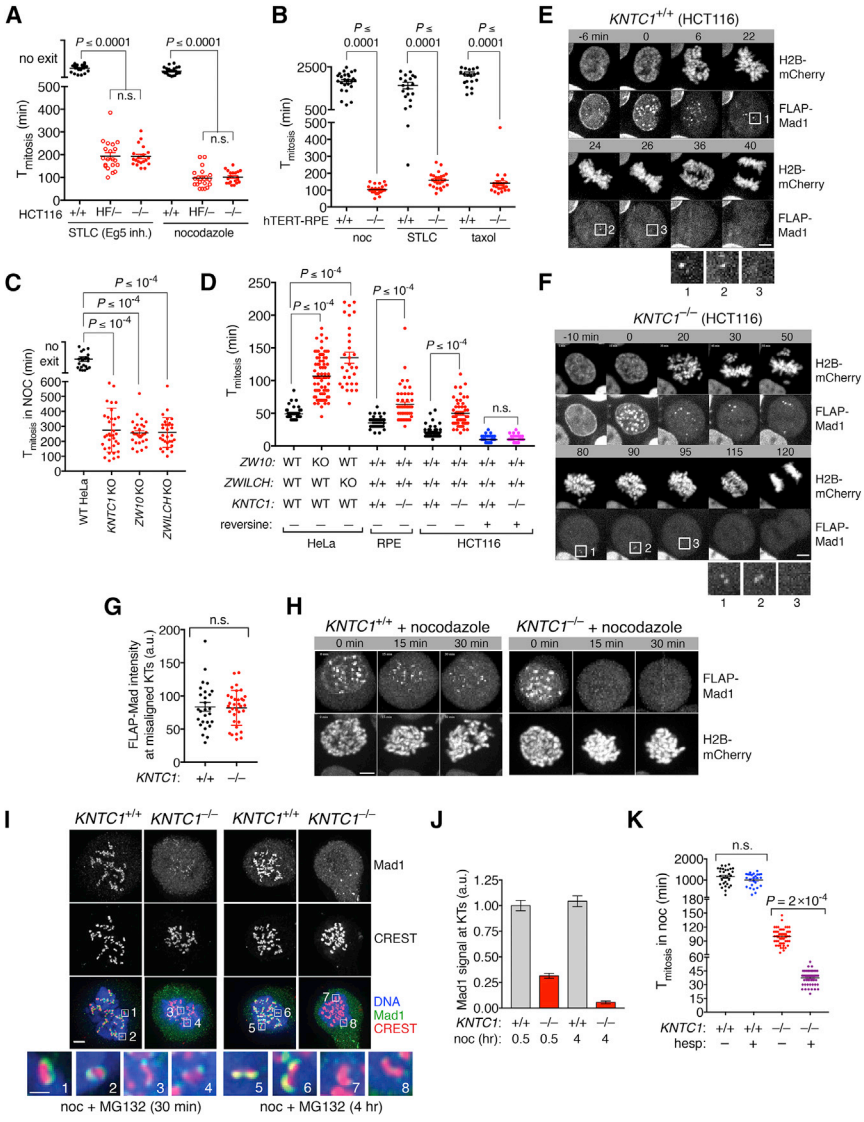

Figure 1. A Temporal Switch in the Requirements for Mad1-Mad2 Targeting to Kinetochores during SAC Signaling

(A) AAV- and CRISPR-mediated genome editing was used to modify the *KNTC1* locus in HCT116 cells (Figures S1A–S1E). Cells expressing H2B-mCherry were treated with nocodazole or STLC and were followed using epifluorescence and differential interference contrast (DIC) time-lapse microscopy. Images were acquired at 10-min intervals. Mitotic duration (from NEBD to chromatin decondensation) was quantified in at least 25 cells per condition per experiment (N = 2). p values were computed using Kruskal-Wallis and Dunn's multiple comparisons tests. Error bars throughout the paper indicate SEM unless stated otherwise.

(B) Wild-type and *KNTC1*$^{-/-}$ RPE1 cells (Figures S1F–S1I) were treated with nocodazole, STLC, or taxol and were followed using DIC optics. Cell rounding (mitotic entry) and cortical blebbing and flattening (mitotic exit) were used as landmarks.

(C) Clonal HeLa *KNTC1*, *ZW10*, and *ZWILCH* knockouts [14] were treated with nocodazole and were followed as in (B).

(D) Mitotic timing in unperturbed wild-type and RZZ-deficient HeLa, RPE, and HCT116 cells. Where indicated, Mps1 kinase was inhibited with reversine.

(E and F) Wild-type and *KNTC1*$^{-/-}$ HCT116 cells expressing H2B-mCherry and FLAP-Mad1 were filmed during unperturbed mitosis using spinning disk confocal microscopy. Insets show enlarged views of FLAP-Mad1 recruitment to and dissociation from kinetochores. Scale bars throughout the paper are 10 μm unless stated otherwise. See also Videos S1 and S2.

(G) Quantification of FLAP-Mad1 at misaligned chromosomes in (E) and (F).

(H) Cells in (E) and (F) were filmed in the presence of nocodazole (n = 6 for wild-type and n = 14 for *KNTC1*$^{-/-}$).

(I and J) Wild-type and *KNTC1*-null RPE cells were treated with nocodazole and MG132 for 30 min or 4 hr before fixation for IFM. Mad1/CREST fluorescence intensity ratios were determined for at least 100 kinetochores in five cells per condition (N = 3).

(K) Wild-type and *KNTC1*-null RPE cells were treated with nocodazole in the presence or absence of hesperadin (hesp) to inhibit Aurora B kinase. Mitotic duration was determined from 30 cells per condition.

See also Figure S1.

(Figures 1F and 1G and Video S2; n = 14 cells). We conclude that early mitotic cells can recruit Mad1-Mad2 to kinetochores and inhibit anaphase onset in the absence of the RZZ complex.

Next, we analyzed Mad1 dynamics in cells undergoing nocodazole-induced SAC arrest. Mad1 initially localized to kinetochores at NEBD in both wild-type and *KNTC1*$^{-/-}$ cells, but this localization was not persistently maintained in the absence of RZZ (Figure 1H). To confirm this result for endogenous Mad1, we treated wild-type and *KNTC1*$^{-/-}$ RPE cells with nocodazole and MG132 (to block mitotic exit) for 30 min or 4 hr and then fixed and analyzed them by immunofluorescence microscopy (IFM). In wild-type cells, Mad1 formed large crescents that were stable over time, whereas it formed compact foci in *KNTC1*$^{-/-}$ cells that were eventually lost from kinetochores (Figures 1I and 1J). Suppression of early mitotic Mad1-Mad2 recruitment by treatment with Aurora B inhibitors [16, 17] eliminated the residual SAC response in *KNTC1*$^{-/-}$ cells ($T_{mitosis}$ = 39 ± 10 min; Figure 1K). These results reveal a temporal switch from RZZ-independent to RZZ-dependent recruitment of Mad1-Mad2 during chronic SAC signaling.

Mps1 Promotes Kinetochore Expansion by Phosphorylating the N Terminus of Rod

Mad1-Mad2 and RZZ localize to the fibrous corona, a phospho-dependent expansion of the outermost kinetochore layer that persists until end-on microtubule attachments are formed [5, 6, 18]. Kinetochore expansion is thought to accelerate mitotic "search and capture" by promoting lateral microtubule attachment [4] and to enhance SAC signaling [5]. RZZ is closely related to endomembrane coatomers that form oligomeric lattices [19, 20] and is

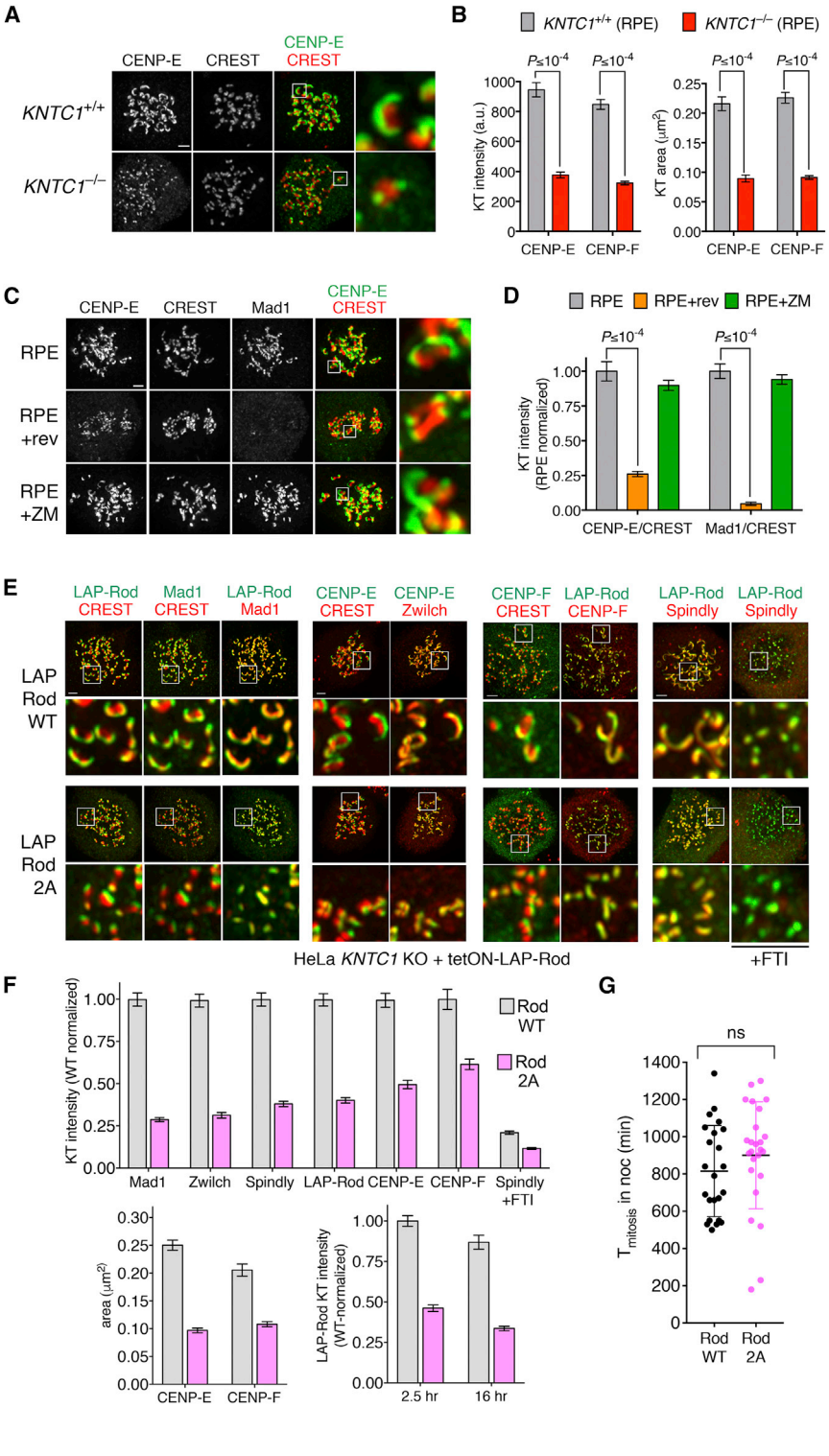

Figure 2. Mps1 Phosphorylation at the N Terminus of Rod Triggers RZZ-Dependent Kinetochore Expansion

(A and B) Wild-type and *KNTC1*$^{-/-}$ RPE cells were treated with nocodazole and MG132 for 2.5 hr before IFM with antibodies to CENP-E (A) or CENP-F (Figure S2A). Crescent size and intensity (B) were quantified in five to ten cells (N = 3).

(C and D) RPE cells were treated with nocodazole and MG132 for 2 hr, after which reversine (rev) or Aurora B inhibitor ZM447439 (ZM) was added or omitted for 1 hr (n = 10 cells, N = 3). Kinetochore-associated Mad1 and CENP-E were visualized by IFM (C) and quantified (D).

(E and F) *KNTC1*-null HeLa cells reconstituted with LAP-Rod^{WT} or LAP-Rod^{2A} were treated with nocodazole for 2.5 hr. IFM was used to visualize crescents (E) and quantify kinetochore-associated LAP-Rod, Mad1, CENP-E, CENP-F, Spindly, and CREST (F) (n = 100 kinetochores in five cells each, N = 2). Where indicated, cells were treated with the farnesyltransferase inhibitor FTI-288 (FTI) as a positive control for blockade of Spindly targeting to kinetochores [25, 26]. Note that kinetochores in LAP-Rod^{2A} cells remained compact during long-term SAC arrest (16 hr nocodazole treatment).

(G) The duration of mitotic arrest in nocodazole-treated LAP-Rod^{WT} and LAP-Rod^{2A} cells was determined by DIC time lapse (n ≥ 50 cells, N = 2) and compared using the Mann-Whitney U test. See also Figure S2.

most likely a "building block" of the corona itself [13, 15, 21, 22]. Consistent with these proposals, two other corona-associated proteins (CENP-E [23] and CENP-F [24]) did not form crescents in *KNTC1*$^{-/-}$ cells (Figures 2A, 2B, and S2A). To ensure that these results reflected loss of kinetochore expansion and not protein mislocalization, we performed correlative light-electron microscopy in cells expressing CENP-A-GFP as a centromere marker. Serial sectioning revealed circumferential expansion of trilaminar plates and fibrous material in wild-type cells (n = 14 kinetochores), whereas the kinetochores of *KNTC1*$^{-/-}$ cells appeared as compact discs (n = 15; Figure S2B) [13]. We conclude that the RZZ complex is required for fibrous corona formation.

In parallel, we looked for mitotic kinases that might activate RZZ for kinetochore expansion. We found that CENP-E kinetochore crescents become compact after treating cells with an Mps1 inhibitor, but not after treatment with an Aurora B inhibitor (Figures 2C and 2D) [13]. Through global phosphoproteomic screening, we identified two Mps1-modified sites at the N terminus of Rod (T13 and S15), upstream of its β-propeller domain [27]. To test the function of these sites, we expressed wild-type (WT) and nonphosphorylatable (2A) versions of Rod in T-Rex FLP-in HeLa cells as LAP (EGFP-TEV-S-peptide) fusions (Figure S2C). Both LAP-Rod^{WT} and LAP-Rod^{2A} were incorporated into the full RZZ complex based on co-immunoprecipitation assays (Figure S2D). We then disrupted the *KNTC1* locus in these cells using CRISPR/Cas9 and isolated transgene-complemented clones. Although LAP-Rod^{WT} and LAP-Rod^{2A} both localized to unattached kinetochores in the absence of

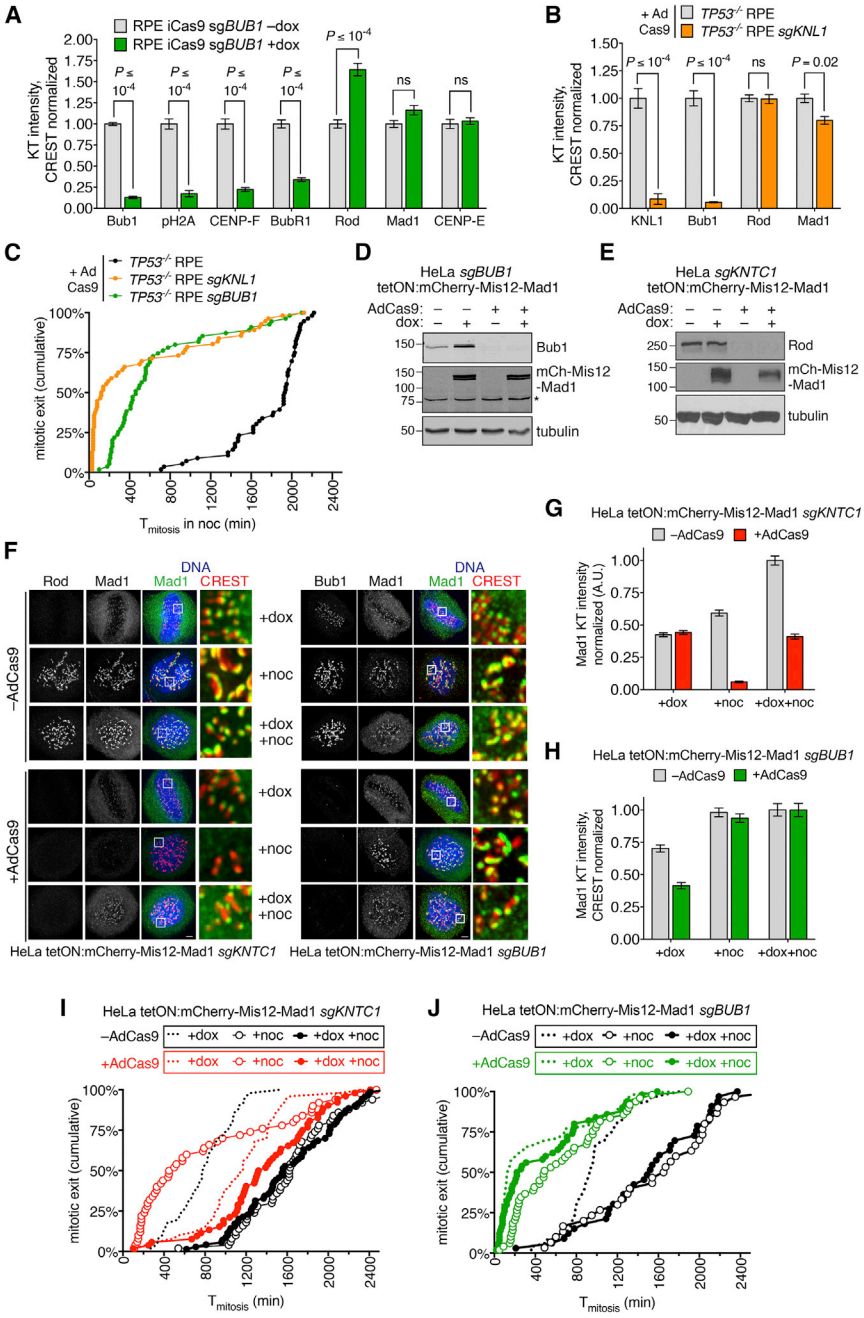

Figure 3. RZZ and Bub1-KNL1 Have Distinct Roles in Recruiting and Activating Mad1-Mad2 at Kinetochores during SAC Signaling

(A) RPE iCas9 cells expressing *sgBUB1* were treated with or without doxycycline and analyzed by IFM after 5 days (for images, see Figure S3A).

(B) *TP53*$^{-/-}$ RPE cells with or without *sgKNL1* were treated with AdCas9 and analyzed by IFM after three days (for images, see Figure S3B).

(C) AdCas9-treated cells were filmed in the presence of nocodazole for 48 hr. Cumulative frequency of mitotic exit is plotted.

(D and E) HeLa cells expressing *BUB1*- or *KNTC1*-specific synthetic guide RNAs (sgRNAs) targeting *BUB1* (D) or *KNTC1* (E) were treated with AdCas9. After 3 days, mCherry-Mis12-Mad1 was induced with doxycycline for 17 hr. Protein depletion or expression was confirmed by western blotting.

(F–H) Cells in (D) and (E) were analyzed by IFM, either with or without a further 3-hr treatment with nocodazole (F). Mad1/CREST ratios were determined for ≥100 kinetochores in acute *KNTC1* (G) and acute *BUB1* (H) knockout cells.

(I and J) Acute *KNTC1* knockouts (I) and acute *BUB1* knockouts (J) were treated with doxycycline and/or nocodazole and followed using DIC time lapse (n ≥ 50 cells, N = 2).

See also Figure S3.

Mad1-Mad2 Requires a Non-receptor Activity of Bub1 to Inhibit Anaphase

Bub1 is required for kinetochore expansion in *Xenopus* egg extracts [5], but its role in fibrous corona formation in human cells has not been examined. Bub1's role in the SAC also remains controversial, with inconsistent results across studies [7–12]. To test Bub1's contribution to these aspects of kinetochore structure and function, we deleted *BUB1* in RPE cells via doxycycline-inducible CRISPR/Cas9 [14]. *BUB1*$^{-/-}$ cells treated with nocodazole formed kinetochore crescents containing Rod, CENP-E, and Mad1, but not CENP-F [12] (Figures 3A and S3A). To ensure complete depletion and avoid postmitotic arrest [14], we deleted *BUB1* or its kinetochore scaffold *KNL1* [1, 2] in p53-deficient RPE cells. *KNL1*$^{-/-}$ cells formed crescents with normal levels of RZZ but slightly less Mad1 (22% reduction; Figures 3B and S3B). However deletion of *BUB1* or *KNL1* decreased the period of nocodazole-induced mitotic arrest by 76% and 93% (median $T_{mitosis}$ = 130 min for *KNL1*$^{-/-}$ cells and 460 min for *BUB1*$^{-/-}$ cells, versus 1,935 min for control cells), indicating that that SAC signaling was functionally compromised.

Although kinetochores in *BUB1*$^{-/-}$ and *KNL1*$^{-/-}$ cells have high levels of Mad1-Mad2, we could not exclude the possibility that a small but functionally important pool was missing. Therefore, we tested the consequences of combining deletion of endogenous Rod, only LAP-Rod^{WT} formed crescents (Figures 2E and 2F). Thus far the only post-translational modification known to be required for crescent formation is C-terminal farnesylation of Spindly, which enables its kinetochore recruitment via interaction with Rod's β-propeller domain [15, 21, 25, 26]. However Rod^{2A} recruited Spindly and other corona-associated proteins in proportion to its own reduced abundance (Figure 2F). Despite having lower levels of Mad1-Mad2, the compact kinetochores in Rod^{2A} cells sustained mitotic arrest in nocodazole as effectively as those in Rod^{WT} cells (Figure 2G). We conclude that Rod's N-terminal phosphorylation is required for fibrous corona formation but not SAC signaling.

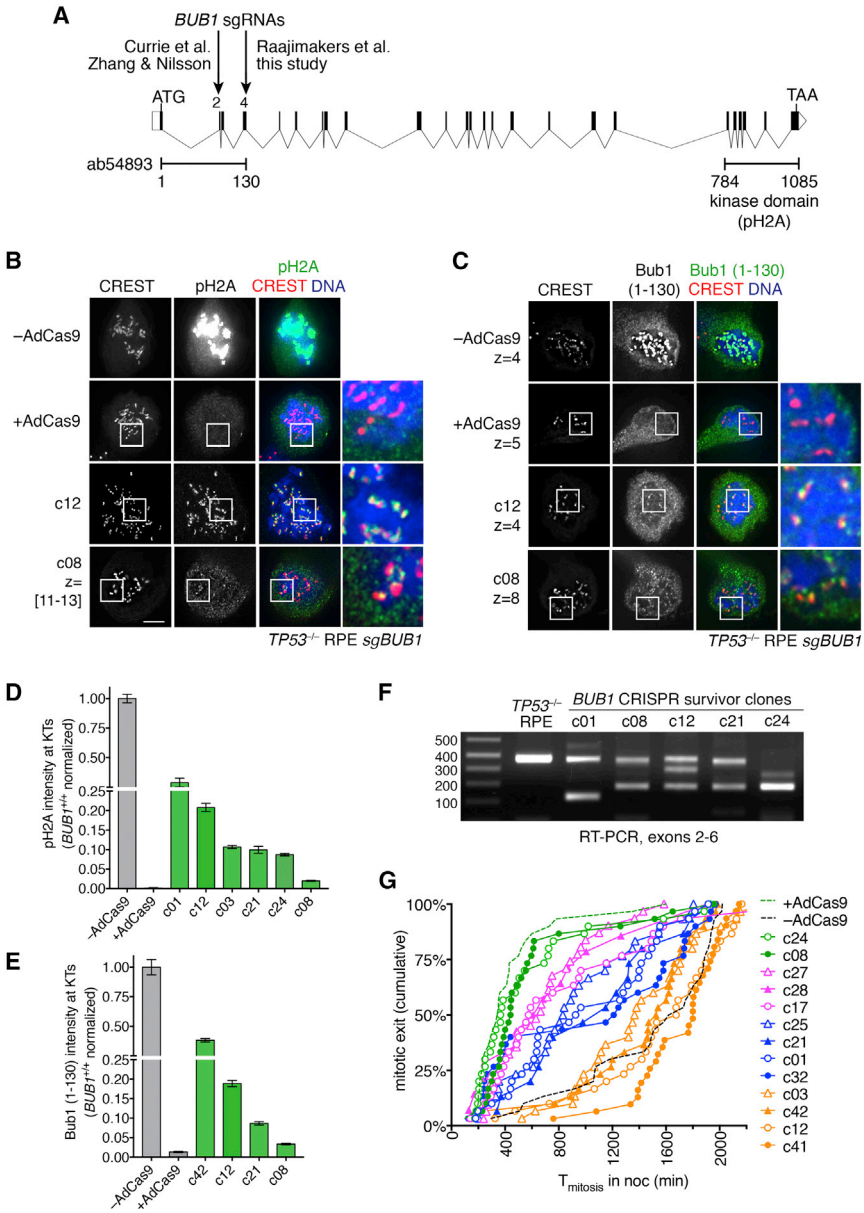

Figure 4. *BUB1*-Disrupted Clones Regain Bub1 Expression and SAC Function through Nonsense-Associated Alternative Splicing

(A) Structure of the *BUB1* locus. Locations of guide RNAs used in this and previous studies [33–35] are shown. Regions encoding N-terminal Bub1 antibody epitope and C-terminal kinase domain are indicated.

(B–E) Parental *TP53*$^{-/-}$ RPE cells (–AdCas9), acute *BUB1* knockout cells (+AdCas9), and *BUB1*-disrupted clones (c12 and c08) were treated with nocodazole and MG132 for 2 hr. Centromeric H2A phosphorylation (B) and kinetochore-associated Bub1 (C) were quantified (D and E, respectively) by IFM (n = 100 kinetochores in 5 cells, N = 2). Where indicated, individual z slices or maximum-intensity projections of adjacent z slices are displayed. For all other images, maximum-intensity projections of full z series are shown.

(F) RNA samples were reverse-transcribed and amplified with PCR primers spanning exons 2–6.

(G) *BUB1*-disrupted clones were treated with nocodazole and were followed using DIC time lapse. Parental *TP53*$^{-/-}$ RPE cells (–AdCas9) and acute *BUB1* knockout cells (+AdCas9) were used as controls.

See also Figure S4 and Data S1.

BUB1 or *KNTC1* with expression of a constitutively kinetochore-bound form of Mad1 (Mis12-Mad1) that is refractory to SAC silencing at metaphase [28] (Figures 3D–3J). Mis12-Mad1 expression triggered a mitotic arrest in *KNTC1*$^{-/-}$ cells that was even longer (median $T_{mitosis}$ = 1170 min) than that observed in wild-type cells expressing Mis12-Mad1 (median $T_{mitosis}$ = 780 min; Figure 3I). This hyperactive response most likely reflects RZZ's role in stripping Mad1 and other SAC mediators from metaphase kinetochores via dynein-dependent transport [29–31]. In contrast *BUB1*$^{-/-}$ cells had a much weaker response to Mis12-Mad1 kinetochore tethering (median $T_{mitosis}$ = 130 min; Figure 3J). We next combined Mis12-Mad1 expression with nocodazole treatment to eliminate dynein-dependent stripping and engage upstream SAC signaling. This regimen further extended the mitotic arrest in *KNTC1*$^{-/-}$ cells (median $T_{mitosis}$ = 1,355 min, versus 1,560 min for wild-type cells) but accelerated mitotic exit in *BUB1*$^{-/-}$ cells (median $T_{mitosis}$ = 240 min) relative to nocodazole treatment alone (median $T_{mitosis}$ = 460 min; Figures 3I and 3J). We conclude that Mad1-Mad2 kinetochore tethering can bypass RZZ, but not Bub1, with respect to SAC signaling. Our findings suggest that RZZ's crucial and most likely sole function in SAC activation is to maintain Mad1-Mad2 at kinetochores, whereas RZZ-dependent corona formation is not required. In contrast Bub1 is not required for RZZ to localize at kinetochores, form the fibrous corona, or recruit Mad1-Mad2. However, Mad1-Mad2 still requires a non-receptor activity of Bub1 to generate a "wait anaphase" signal.

BUB1-Disrupted Clones Re-express Bub1 and Regain SAC Function via Nonsense-Associated Alternative Splicing

The SAC defect that we observed after acute *BUB1* disruption is consistent with studies in *Bub1* conditional-knockout mouse embryonic fibroblasts [9, 32], but not with recent studies in *BUB1*-disrupted human cell clones [33–35] (Figure 4A). To understand the basis of this discrepancy, we isolated 13 clones after acute disruption of *BUB1* in p53-deficient RPE cells. All clones exhibited a partial (3%–30%) recovery of Bub1 expression, kinetochore localization, and H2A kinase activity as judged by IFM with antibodies that recognize Bub1's N terminus and T120-phosphorylated H2A (Figures 4B–4E). We performed

RT-PCR and sequencing on five clones (Figure 4F and Data S1). Full-length *BUB1* transcripts harbored exon 4 indels that induce frameshift and early termination (Figure S4A). We also observed shorter transcripts that skipped part or all of exon 4 and/or utilized cryptic splice sites (Figures S4B–S4F). A number of alternatively spliced transcripts encoded *BUB1* open reading frames (ORFs) with short N-terminal deletions or insertions, thus explaining Bub1 re-expression (Figures S4C–S4F). Eleven of 13 clones exhibited partial or complete recovery of SAC function relative to acute deletion of *BUB1* (Figure 4G). Among the five clones analyzed by RT-PCR and sequencing, clone 12 was fully SAC proficient and had the highest rate of in-frame transcripts (6 of 36), whereas clone 21 had intermediate SAC function and a lesser rate (3 of 31). No in-frame transcripts were identified in clone 8 (0 of 18) and clone 24 (0 of 21), which were the most SAC defective (Figure 4G). Taken together, these results suggest that nonsense-associated alternative splicing (NAS) [36] attenuates and in some cases suppresses the effects of null mutations in *BUB1*. Our findings demonstrate how genome editing can trigger both acute loss of function and compensatory changes in mRNA structure that result in phenocopying of unedited cells.

DISCUSSION

In cells treated with spindle poisons, Mad1-Mad2 remains bound to kinetochores and catalyzes MCC production for 1,000 min or more, thus extending mitosis at least 30-fold. How (and why) this sustained response occurs is not well understood. In yeast, Bub1 is the sole receptor for Mad1-Mad2 and required for the SAC [37], but models for Mad1-Mad2 regulation in mammalian cells differ considerably [7–12]. In our studies, acute *BUB1* or *KNL1* deletion led to SAC failure despite high levels of Mad1-Mad2 at kinetochores. Furthermore *BUB1*$^{-/-}$ cells were largely unresponsive to Mis12-Mad1, which is constitutively tethered to kinetochores and cannot be silenced at metaphase. Similar results were obtained independently using a Ndc80-Mad1 fusion [35]. These data strongly suggest a non-receptor function of Bub1-KNL1 that is required for kinetochore-bound Mad1-Mad2 to inhibit anaphase. One possibility is that Bub1 functions as a co-catalyst in MCC assembly by recruiting Cdc20 to kinetochores [7, 38]. Asking whether this occurs *in vivo* will require SAC-independent methods for synchronizing *BUB1*$^{-/-}$ and *KNL1*$^{-/-}$ cells in mitosis in sufficient quantity and purity for biochemical studies of MCC assembly [39] or tools for rapidly eliminating Bub1 and KNL1 after SAC-dependent synchronization.

Our studies also shed light on RZZ's role in the SAC. By tracking Mad1 dynamics with high temporal resolution, we demonstrate that kinetochores in early mitotic cells can recruit Mad1-Mad2 without RZZ and can delay anaphase onset by 100–300 min, thus mitigating the impact of less efficient chromosome congression in RZZ-null cells. However kinetochores with attachment defects that persist beyond this timeframe require RZZ to recruit Mad1-Mad2 and maintain SAC arrest. Expression of Mis12-Mad1 reinstated long-term arrest in *KNTC1*$^{-/-}$ cells, suggesting that RZZ's crucial and perhaps only role in the SAC is to tether Mad1-Mad2 to kinetochores. It has been proposed that RZZ mediates SAC signaling at unattached, but not tensionless, kinetochores [10]. However, *KNTC1*$^{-/-}$ cells challenged with spindle poisons that block attachment (nocodazole) or permit attachment without tension (STLC and taxol) escaped SAC arrest with similar kinetics (Figure 1B).

RZZ is also implicated in formation of the fibrous corona, a structural expansion of the outer kinetochore that precedes microtubule attachment [4, 6, 18]. Kinetochore expansion depends on mitotic kinases [5, 13], but relevant phosphorylation events are not known. We identified two Mps1-regulated phosphosites just upstream of Rod's β-propeller domain [27] that are required for kinetochore expansion, but not SAC arrest. Rod and Spindly not only interact via this domain [15, 21], but also inhibit their own assembly into polymers [13, 40]. Together, these findings suggest that phosphorylation alleviates a structural barrier to Spindly-RZZ polymerization.

In this study and others [3, 14, 39, 41, 42], we used genome editing to delete or disrupt exons of genes involved in cell division. Normally this results in a "knockout" because of nonsense-mediated decay (NMD), a pathway that degrades mRNAs with premature termination codons (PTCs) [43, 44]. However PTCs can also trigger NAS, a less-well-understood pathway in which splicing rules are relaxed to bypass the PTC and restore expression of near-full length ORFs [36, 45, 46]. NAS could also explain why *BUB1* exon-2-disrupted HeLa cells manifest a clear SAC defect after *BUB1* exon-8-specific RNAi [35]. In conclusion, NMD and NAS have opposite effects on the expressivity and penetrance of nonsense mutations and should not be overlooked in the design, analysis, and interpretation of genome editing experiments.

STAR★METHODS

Detailed methods are provided in the online version of this paper and include the following:

- KEY RESOURCES TABLE
- CONTACT FOR REAGENT AND RESOURCE SHARING
- EXPERIMENTAL MODEL AND SUBJECT DETAILS
  - Cell lines and chemicals
- METHOD DETAILS
  - Transgene expression
  - AAV-mediated gene targeting
  - CRISPR/Cas9-mediated genome editing
  - Immunofluorescence microscopy and live-cell imaging
  - Correlative light-electron microscopy
  - Cell lysis, immunoprecipitation, and western blotting
  - RT-PCR and sequencing
- QUANTIFICATION AND STATISTICAL ANALYSIS

SUPPLEMENTAL INFORMATION

Supplemental Information includes four figures, two videos, and one data file and can be found with this article online at https://doi.org/10.1016/j.cub.2018.10.006.

ACKNOWLEDGMENTS

We thank George Church, Didier Trono, David Sabatini, and Feng Zhang for sharing plasmids through Addgene. The authors were supported by grants from the National Institutes of Health (R01GM094972, P30CA008748,

R01GM059363, and R35GM126930) and the Harold G. and Leila Y. Mathers Charitable Foundation.

AUTHOR CONTRIBUTIONS

J.-A.R.-R., C.L., K.L.M., J.C., J.M., and P.V.J. performed molecular biology, cell imaging, and biochemical studies and analyzed data. V.S. performed electron microscopy and analyzed data. A.K., I.M.C., and P.V.J. planned and supervised the research, analyzed data, and secured funding. J.-A.R.-R. and P.V.J. wrote the paper with input from all authors.

DECLARATION OF INTERESTS

The authors declare no competing interests.

Received: April 4, 2018
Revised: August 30, 2018
Accepted: October 2, 2018
Published: October 25, 2018

REFERENCES

1. London, N., and Biggins, S. (2014). Signalling dynamics in the spindle checkpoint response. Nat. Rev. Mol. Cell Biol. *15*, 736–747.
2. Musacchio, A. (2015). The molecular biology of spindle assembly checkpoint signaling dynamics. Curr. Biol. *25*, R1002–R1018.
3. Rodriguez-Bravo, V., Maciejowski, J., Corona, J., Buch, H.K., Collin, P., Kanemaki, M.T., Shah, J.V., and Jallepalli, P.V. (2014). Nuclear pores protect genome integrity by assembling a premitotic and Mad1-dependent anaphase inhibitor. Cell *156*, 1017–1031.
4. Magidson, V., Paul, R., Yang, N., Ault, J.G., O'Connell, C.B., Tikhonenko, I., McEwen, B.F., Mogilner, A., and Khodjakov, A. (2015). Adaptive changes in the kinetochore architecture facilitate proper spindle assembly. Nat. Cell Biol. *17*, 1134–1144.
5. Wynne, D.J., and Funabiki, H. (2015). Kinetochore function is controlled by a phospho-dependent coexpansion of inner and outer components. J. Cell Biol. *210*, 899–916.
6. Hoffman, D.B., Pearson, C.G., Yen, T.J., Howell, B.J., and Salmon, E.D. (2001). Microtubule-dependent changes in assembly of microtubule motor proteins and mitotic spindle checkpoint proteins at PtK1 kinetochores. Mol. Biol. Cell *12*, 1995–2009.
7. Vleugel, M., Hoek, T.A., Tromer, E., Sliedrecht, T., Groenewold, V., Omerzu, M., and Kops, G.J. (2015). Dissecting the roles of human BUB1 in the spindle assembly checkpoint. J. Cell Sci. *128*, 2975–2982.
8. Klebig, C., Korinth, D., and Meraldi, P. (2009). Bub1 regulates chromosome segregation in a kinetochore-independent manner. J. Cell Biol. *185*, 841–858.
9. Zhang, G., Lischetti, T., Hayward, D.G., and Nilsson, J. (2015). Distinct domains in Bub1 localize RZZ and BubR1 to kinetochores to regulate the checkpoint. Nat. Commun. *6*, 7162.
10. Silió, V., McAinsh, A.D., and Millar, J.B. (2015). KNL1-Bubs and RZZ provide two separable pathways for checkpoint activation at human kinetochores. Dev. Cell *35*, 600–613.
11. Caldas, G.V., Lynch, T.R., Anderson, R., Afreen, S., Varma, D., and DeLuca, J.G. (2015). The RZZ complex requires the N-terminus of KNL1 to mediate optimal Mad1 kinetochore localization in human cells. Open Biol. *5*, 150160.
12. Raaijmakers, J.A., van Heesbeen, R.G.H.P., Blomen, V.A., Janssen, L.M.E., van Diemen, F., Brummelkamp, T.R., and Medema, R.H. (2018). BUB1 is essential for the viability of human cells in which the spindle assembly checkpoint is compromised. Cell Rep. *22*, 1424–1438.
13. Sacristan, C., Ahmad, M.U.D., Keller, J., Fermie, J., Groenewold, V., Tromer, E., Fish, A., Melero, R., Carazo, J.M., Klumperman, J., et al. (2018). Dynamic kinetochore size regulation promotes microtubule capture and chromosome biorientation in mitosis. Nat. Cell Biol. *20*, 800–810.
14. McKinley, K.L., and Cheeseman, I.M. (2017). Large-scale analysis of CRISPR/Cas9 cell-cycle knockouts reveals the diversity of p53-dependent responses to cell-cycle defects. Dev. Cell *40*, 405–420.e2.
15. Gama, J.B., Pereira, C., Simões, P.A., Celestino, R., Reis, R.M., Barbosa, D.J., Pires, H.R., Carvalho, C., Amorim, J., Carvalho, A.X., et al. (2017). Molecular mechanism of dynein recruitment to kinetochores by the Rod-Zw10-Zwilch complex and Spindly. J. Cell Biol. *216*, 943–960.
16. Saurin, A.T., van der Waal, M.S., Medema, R.H., Lens, S.M., and Kops, G.J. (2011). Aurora B potentiates Mps1 activation to ensure rapid checkpoint establishment at the onset of mitosis. Nat. Commun. *2*, 316.
17. Santaguida, S., Vernieri, C., Villa, F., Ciliberto, A., and Musacchio, A. (2011). Evidence that Aurora B is implicated in spindle checkpoint signalling independently of error correction. EMBO J. *30*, 1508–1519.
18. McEwen, B.F., Arena, J.T., Frank, J., and Rieder, C.L. (1993). Structure of the colcemid-treated PtK1 kinetochore outer plate as determined by high voltage electron microscopic tomography. J. Cell Biol. *120*, 301–312.
19. Schmitt, H.D. (2010). Dsl1p/Zw10: common mechanisms behind tethering vesicles and microtubules. Trends Cell Biol. *20*, 257–268.
20. Civril, F., Wehenkel, A., Giorgi, F.M., Santaguida, S., Di Fonzo, A., Grigorean, G., Ciccarelli, F.D., and Musacchio, A. (2010). Structural analysis of the RZZ complex reveals common ancestry with multisubunit vesicle tethering machinery. Structure *18*, 616–626.
21. Mosalaganti, S., Keller, J., Altenfeld, A., Winzker, M., Rombaut, P., Saur, M., Petrovic, A., Wehenkel, A., Wohlgemuth, S., Müller, F., et al. (2017). Structure of the RZZ complex and molecular basis of its interaction with Spindly. J. Cell Biol. *216*, 961–981.
22. Basto, R., Scaerou, F., Mische, S., Wojcik, E., Lefebvre, C., Gomes, R., Hays, T., and Karess, R. (2004). In vivo dynamics of the rough deal checkpoint protein during Drosophila mitosis. Curr. Biol. *14*, 56–61.
23. Cooke, C.A., Schaar, B., Yen, T.J., and Earnshaw, W.C. (1997). Localization of CENP-E in the fibrous corona and outer plate of mammalian kinetochores from prometaphase through anaphase. Chromosoma *106*, 446–455.
24. Rattner, J.B., Rao, A., Fritzler, M.J., Valencia, D.W., and Yen, T.J. (1993). CENP-F is a. ca 400 kDa kinetochore protein that exhibits a cell-cycle dependent localization. Cell Motil. Cytoskeleton *26*, 214–226.
25. Holland, A.J., Reis, R.M., Niessen, S., Pereira, C., Andres, D.A., Spielmann, H.P., Cleveland, D.W., Desai, A., and Gassmann, R. (2015). Preventing farnesylation of the dynein adaptor Spindly contributes to the mitotic defects caused by farnesyltransferase inhibitors. Mol. Biol. Cell *26*, 1845–1856.
26. Moudgil, D.K., Westcott, N., Famulski, J.K., Patel, K., Macdonald, D., Hang, H., and Chan, G.K. (2015). A novel role of farnesylation in targeting a mitotic checkpoint protein, human Spindly, to kinetochores. J. Cell Biol. *208*, 881–896.
27. Maciejowski, J., Drechsler, H., Grundner-Culemann, K., Ballister, E.R., Rodriguez-Rodriguez, J.A., Rodriguez-Bravo, V., Jones, M.J.K., Foley, E., Lampson, M.A., Daub, H., et al. (2017). Mps1 regulates kinetochore-microtubule attachment stability via the Ska complex to ensure error-free chromosome segregation. Dev. Cell *41*, 143–156.e6.
28. Maldonado, M., and Kapoor, T.M. (2011). Constitutive Mad1 targeting to kinetochores uncouples checkpoint signalling from chromosome biorientation. Nat. Cell Biol. *13*, 475–482.
29. Gassmann, R., Holland, A.J., Varma, D., Wan, X., Civril, F., Cleveland, D.W., Oegema, K., Salmon, E.D., and Desai, A. (2010). Removal of Spindly from microtubule-attached kinetochores controls spindle checkpoint silencing in human cells. Genes Dev. *24*, 957–971.
30. Howell, B.J., McEwen, B.F., Canman, J.C., Hoffman, D.B., Farrar, E.M., Rieder, C.L., and Salmon, E.D. (2001). Cytoplasmic dynein/dynactin drives kinetochore protein transport to the spindle poles and has a role in mitotic spindle checkpoint inactivation. J. Cell Biol. *155*, 1159–1172.
31. Silva, P.M., Reis, R.M., Bolanos-Garcia, V.M., Florindo, C., Tavares, A.A., and Bousbaa, H. (2014). Dynein-dependent transport of spindle assembly

checkpoint proteins off kinetochores toward spindle poles. FEBS Lett. *588*, 3265–3273.

32. Perera, D., Tilston, V., Hopwood, J.A., Barchi, M., Boot-Handford, R.P., and Taylor, S.S. (2007). Bub1 maintains centromeric cohesion by activation of the spindle checkpoint. Dev. Cell *13*, 566–579.
33. Currie, C.E., Mora-Santos, M.D., Smith, C.A., McAinsh, A.D., and Millar, J.B. (2018). Bub1 is not essential for the checkpoint response to unattached kinetochores in diploid human cells. Curr. Biol. *28*, R929–R930.
34. Raaijmakers, J.A., Tanenbaum, M.E., Maia, A.F., and Medema, R.H. (2009). RAMA1 is a novel kinetochore protein involved in kinetochore-microtubule attachment. J. Cell Sci. *122*, 2436–2445.
35. Zhang, G., Kruse, T., and Nilsson, J. (2018). The RZZ complex facilitates Mad1 binding to Bub1 ensuring efficient checkpoint signaling. bioRxiv. https://doi.org/10.1101/322834.
36. Cartegni, L., Chew, S.L., and Krainer, A.R. (2002). Listening to silence and understanding nonsense: exonic mutations that affect splicing. Nat. Rev. Genet. *3*, 285–298.
37. London, N., and Biggins, S. (2014). Mad1 kinetochore recruitment by Mps1-mediated phosphorylation of Bub1 signals the spindle checkpoint. Genes Dev. *28*, 140–152.
38. Faesen, A.C., Thanasoula, M., Maffini, S., Breit, C., Müller, F., van Gerwen, S., Bange, T., and Musacchio, A. (2017). Basis of catalytic assembly of the mitotic checkpoint complex. Nature *542*, 498–502.
39. Maciejowski, J., George, K.A., Terret, M.E., Zhang, C., Shokat, K.M., and Jallepalli, P.V. (2010). Mps1 directs the assembly of Cdc20 inhibitory complexes during interphase and mitosis to control M phase timing and spindle checkpoint signaling. J. Cell Biol. *190*, 89–100.
40. Pereira, C., Reis, R.M., Gama, J.B., Celestino, R., Cheerambathur, D.K., Carvalho, A.X., and Gassmann, R. (2018). Self-assembly of the RZZ complex into filaments drives kinetochore expansion in the absence of microtubule attachment. Curr. Biol. Published online October 25, 2018. https://doi.org/10.1016/j.cub.2018.08.056.
41. Tsou, M.-F.B., Wang, W.-J., George, K.A., Uryu, K., Stearns, T., and Jallepalli, P.V. (2009). Polo kinase and separase regulate the mitotic licensing of centriole duplication in human cells. Dev. Cell *17*, 344–354.
42. McKinley, K.L., Sekulic, N., Guo, L.Y., Tsinman, T., Black, B.E., and Cheeseman, I.M. (2015). The CENP-L-N complex forms a critical node in an integrated meshwork of interactions at the centromere-kinetochore interface. Mol. Cell *60*, 886–898.
43. Popp, M.W., and Maquat, L.E. (2016). Leveraging rules of nonsense-mediated mrna decay for genome engineering and personalized medicine. Cell *165*, 1319–1322.
44. Lykke-Andersen, S., and Jensen, T.H. (2015). Nonsense-mediated mRNA decay: an intricate machinery that shapes transcriptomes. Nat. Rev. Mol. Cell Biol. *16*, 665–677.
45. Anderson, J.L., Mulligan, T.S., Shen, M.C., Wang, H., Scahill, C.M., Tan, F.J., Du, S.J., Busch-Nentwich, E.M., and Farber, S.A. (2017). mRNA processing in mutant zebrafish lines generated by chemical and CRISPR-mediated mutagenesis produces unexpected transcripts that escape nonsense-mediated decay. PLoS Genet. *13*, e1007105.
46. Mou, H., Smith, J.L., Peng, L., Yin, H., Moore, J., Zhang, X.O., Song, C.Q., Sheel, A., Wu, Q., Ozata, D.M., et al. (2017). CRISPR/Cas9-mediated genome editing induces exon skipping by alternative splicing or exon deletion. Genome Biol. *18*, 108.
47. Berdougo, E., Terret, M.E., and Jallepalli, P.V. (2009). Functional dissection of mitotic regulators through gene targeting in human somatic cells. Methods Mol. Biol. *545*, 21–37.
48. Magidson, V., He, J., Ault, J.G., O'Connell, C.B., Yang, N., Tikhonenko, I., McEwen, B.F., Sui, H., and Khodjakov, A. (2016). Unattached kinetochores rather than intrakinetochore tension arrest mitosis in taxol-treated cells. J. Cell Biol. *212*, 307–319.

STAR★METHODS

KEY RESOURCES TABLE

REAGENT or RESOURCE	SOURCE	IDENTIFIER
Antibodies		
CREST (human)	Immunovision	HCT-0100; RRID: AB_2744669
Rod (mouse)	Santa Cruz	sc-81853; RRID: AB_2133542
Zw10 (rabbit)	Abcam	ab21582; RRID: AB_779030
Zwilch (mouse)	A. Musacchio	N/A
Mad1 (mouse)	A. Musacchio	clone BB3-8
Mad2 (rabbit)	Bethyl	A300-301A; RRID: AB_2281536
Bub1 (rabbit)	Genetex	GTX107497; RRID: AB_1949770
Bub1 (mouse)	Abcam	ab54893; RRID: AB_940664
BubR1 (mouse)	BD Biosciences	BD612503; RRID: AB_2066085
KNL1 (rabbit)	Bethyl	A300-804A; RRID: AB_577218
Spindly (rabbit)	Bethyl	A301-354A; RRID: AB_937753
CENP-E (mouse)	Abcam	ab5093; RRID: AB_304747
CENP-F (rabbit)	Novus	NB500-101; RRID: AB_2229328
$p150^{glued}$ (mouse)	BD Biosciences	BD612708; RRID: AB_399947
phospho-T210 H2A (rabbit)	Active Motif	39391; RRID: AB_2744670
phospho-T13/S15 Rod (rabbit)	Jallepalli Lab [27]	N/A
EGFP (mouse)	Santa Cruz	sc-9996; RRID: AB_627695
EGFP (mouse)	ThermoFisher	A-11120 (clone 3E6); RRID: AB_221568
EGFP (rabbit)	Jallepalli Lab [27]	N/A
α-tubulin (mouse)	Santa Cruz	sc-5286; RRID: AB_628411
α-tubulin (rat)	Chemicon	MAB1864 (clone YL1/2); RRID: AB_2210391
mCherry (rabbit)	ThermoFisher	PA5-34974; RRID: AB_2552323
mCherry (mouse)	Abcam	ab125096; RRID: AB_11133266
Bacterial and Virus Strains		
AdCas9	ViraQuest	N/A
Ad5 CMV Cre	Vector Development Lab, Baylor College of Medicine	Lot#032415
Chemicals, Peptides, and Recombinant Proteins		
Nocodazole	Sigma	Cat#M1404; CAS:31430-18-9
Taxol (Paclitaxel)	Sigma	Cat#T7402; CAS:254753-54-3
S-Trityl-L-cysteine (STLC)	ThermoFisher	Cat#2191; CAS:2799-07-7
MG132	Selleckchem	Cat#S2619; CAS:133407-82-6
Hesperidin	Selleckchem	Cat#S2309; CAS:520-26-3
ZM447439	Tocris	Cat#2458; CAS:331771-20-1
Reversine	Cayman Chemical	Cat#10004412; CAS:656820-32-5
FTI-277	Sigma	Cat#F9803; CAS:170006-73-2
G418	Corning	Cat#61234-RF; CAS:108321-42-2
Blasticidin	ThermoFisher	Cat#A1113903; CAS:2079-00-7
Puromycine	ThermoFisher	Cat#A1113803; CAS: 58-58-2
Hygromycin	Calbiochem	Cat#400051; CAS: 31282-04-9
FuGene 6	Promega	Cat#E2691
SuperScript IV First-Strand Synthesis System	ThermoFisher	Cat#18091050
TOPO-TA Cloning Kit	ThermoFisher	Cat#450071

(*Continued on next page*)

Continued

REAGENT or RESOURCE	SOURCE	IDENTIFIER
Experimental Models: Cell Lines		
HEK293	ATCC	CCL-1573
Lenti-X 293T	Clontech	632180
Phoenix-GP293	ATCC	CCL-3215
HCT116	ATCC	CCL-247
HCT116 KNTC1 (HF/+)	this study	N/A
HCT116 KNTC1 (HF/-)	this study	N/A
HCT116 KNTC1 (−/−)	this study	N/A
HeLa	ATCC	CCL-2
HeLa + sgKNTC1	this study	N/A
HeLa TetON-mCherry-Mis12-Mad1	this study	N/A
HeLa TetON-mCherry-Mis12-Mad1 + sgKNTC1	this study	N/A
HeLa TetON-mCherry-Mis12-Mad1 + sgBub1	this study	N/A
HeLa iCas9	Cheeseman Lab [14]	N/A
HeLa iCas9 KNTC1 KO	Cheeseman Lab [14]	Subcloned after sgKNTC1 + dox
HeLa iCas9 ZW10 KO	Cheeseman Lab [14]	Subcloned after sgZW10 + dox
HeLa iCas9 ZWILCH KO	Cheeseman Lab [14]	Subcloned after sgZWILCH + dox
HeLa Flp-In T-Rex	S. Taylor	N/A
HeLa Flp-In T-Rex LAP-Rod WT (KNTC1 KO)	this study	Subcloned after sgKNTC1 + AdCas9
HeLa Flp-In T-Rex LAP-Rod 2A (KNTC1 KO)	this study	Subcloned after sgKNTC1 + AdCas9
RPE1	Clontech	now ATCC CRL-4000
RPE1 KNTC1(−/−)	this study	Subcloned after cotransfection with KNTC1 gRNA vectors (tru1 + tru5) and Cas9
RPE1 iCas9	Cheeseman Lab [14]	N/A
RPE1 iCas9 + sgBUB1	Cheeseman Lab [14]	N/A
RPE1 TP53(−/−)	this study	Subcloned after cotransfection with TP53 gRNA vector and Cas9
RPE1 TP53(−/−) + sgBUB1	this study	N/A
RPE1 TP53(−/−) + sgKNL1	this study	N/A
Recombinant DNA		
pcDNA5/FRT/TO	ThermoFisher	V6520-20
pcDNA5/FRT/TO-LAP-Rod (WT)	this study	N/A
pcDNA5/FRT/TO-LAP-Rod (2A)	this study	N/A
pOG44	ThermoFisher	V6005-20
PB-tetON-mCherry-Mis12-Mad1	this study	N/A
pSuperPiggyBac transposase	System Biosciences	PB210PA-1
pAAV-lacZ	Agilent	AAV Helper-Free System (240071)
pRC	Agilent	AAV Helper-Free System (240071)
pHelper	Agilent	AAV Helper-Free System (240071)
pAAV-KNTC1-HF	this study	N/A
pCAGGS-FLPe	GeneBridges	A201
pVSV-G	Clontech	PT3343-5
pQCXIN-FLAP-Mad1	Jallepalli Lab [3]	N/A
pQCXIB-H2B-mCherry	Jallepalli Lab [3]	N/A
pQCXIB-GFP-CENP-A	this study	N/A
empty gRNA vector	G. Church	Addgene 41824
TP53 gRNA vector; target GGCAGCTACGGTTTCCGTC	M.-F. Tsou	N/A
KNTC1.tru1 gRNA vector; target GTGGCCACTAAACACTTC	this study	N/A

(*Continued on next page*)

Continued

REAGENT or RESOURCE	SOURCE	IDENTIFIER
KNTC1.tru5 gRNA vector; target GTGGACGTTATTCCTAA	this study	N/A
human codon-optimized Cas9	G. Church	Addgene 41815
psPAX2	D. Trono	Addgene 12260
pMD2.G	D. Trono	Addgene 12259
lenti-sgRNA	D. Sabatini	Addgene 71409
lentiguide-puro	F. Zhang	Addgene 52963
lentiguide-puro-sgKNL1; target TAATTTAAAGCTTCACACCG	this study	N/A
lenti-sgKNTC1; target CCCGCCCAGGCAATGTACAG	Cheeseman Lab [14]	N/A
lenti-sgBUB1; target CTTTTCTTGAACCGACACTC	Cheeseman Lab [14]	N/A
lenti-sgZWILCH; target CTTTGCTGATCAACTGCACT	Cheeseman Lab [14]	N/A
lenti-sgZW10; target CAAAACTTCTGTCACGAACG	Cheeseman Lab [14]	N/A
Software and Algorithms		
Zifit	Zinc Finger Consortium	http://zifit.partners.org
sgRNA Designer	Broad Institute	https://www.broadinstitute.org
SoftWoRx	GE Healthcare	https://www.gelifesciences.com
NIS Elements v5.41	Nikon	https://www.nikoninstruments.com, RRID:SCR_014329
ImageJ v1.51	NIH	https://imagej.nih.gov, RRID:SCR_003070
Prism 7.0	GraphPad	https://www.graphpad.com, RRID:SCR_002798
Lasergene v14	DNASTAR	https://www.dnastar.com

CONTACT FOR REAGENT AND RESOURCE SHARING

Further information and requests for resources and reagents should be directed to and will be fulfilled by the Lead Contact, Prasad Jallepalli (jallepap@mskcc.org).

EXPERIMENTAL MODEL AND SUBJECT DETAILS

Cell lines and chemicals

Cell lines used in this study are described in the Key Resources Table. HeLa (human cervical adenocarcinoma, female) and HEK293 (human embryonic kidney, female) derivatives were grown at 37°C in Dulbecco's modified eagle medium (DMEM) with 10% tetracycline free fetal bovine serum, 100 U/mL penicillin, and 100 U/mL streptomycin. hTERT-RPE (human retinal pigment epithelium, female) derivatives were grown at 37°C in a 1:1 mixture of DMEM and Ham's F-12 medium with 10% fetal bovine serum, 100 U/mL penicillin, and 100 U/mL streptomycin, and 2.5 mM L-glutamine. HCT116 (human colorectal adenocarcinoma, male) were grown at 37°C in McCoy's 5A medium with 10% fetal bovine serum, 100 U/mL penicillin, and 100 U/mL streptomycin. Unless stated otherwise, nocodazole (660 nM), taxol (1 μM), S-trityl-L-cysteine (10 μM), MG132 (10 μM), hesperadin (100 nM), ZM447439 (2 μM), reversine (500 nM), and FTI-288 (10 μM) were used at the indicated concentrations.

METHOD DETAILS

Transgene expression

LAP-Rod (WT or 2A) was cloned into pcDNA5/FRT/TO. Constructs were cotransfected with pOG44 into HeLa T-Rex Flp-In cells using FuGene 6 (Roche). Integrants were selected using hygromycin (0.2 mg/mL), picked as single colonies, and induced with doxycycline (0.8 μg/mL). mCherry-Mis12-Mad1 [28] was cloned into a piggyBac vector containing a doxycycline-inducible promoter (*tetON*) and constitutively expressing reverse tetracycline transactivator (*rtTA*) and neomycin phosphotransferase (*neoR*) linked by the self-cleaving T2A peptide. HeLa cells were cotransfected with this construct and pSuperPiggyBac transposase (System Biosciences), selected in G418 (0.5 mg/mL), and induced as above. For stable expression of FLAP-Mad1, EGFP-CENP-A, and H2B-mCherry, retroviral transfer plasmids were cotransfected with pVSV-G into Phoenix 293 cells. For stable expression of mRuby-CENP-A or gene-specific sgRNAs, lentiviral transfer plasmids were cotransfected with psPAX2 and pMD2.G into Lenti-X 293T cells (Clontech). 24 to 48 hr later, supernatants were filtered, mixed 1:1 with fresh medium containing polybrene (20 μg/mL), and applied to target cells for 24 hr. Transductants were selected in G418, blasticidin (5 μg/mL), or puromycin (5 to 20 μg/mL).

AAV-mediated gene targeting

5′ and 3′ homology arms encompassing *KNTC1* exons 2 and 3 were amplified from human BAC clone RP11-18E11 using Pfusion DNA polymerase. A new *loxP* site was added upstream of exon 2 via XbaI digest and linker ligation. The entire targeting construct was transferred to pAAV as a NotI fragment. All manipulated regions were checked by sequencing to ensure their integrity. Procedures for preparing infectious AAV particles, transducing HCT116 cells, and isolating correctly targeted clones were performed as described [47]. The *FRT-neo^{R}-FRT* cassette was excised through transient expression of FLP recombinase (pCAGGS-FLPe) and limiting dilution. To delete *KNTC1^{HF}*, cells were infected with AdCre (Vector Development Laboratory, Baylor College of Medicine).

CRISPR/Cas9-mediated genome editing

Zifit (http://zifit.partners.org/ZiFiT/ChoiceMenu.aspx) and sgRNA Designer (https://www.broadinstitute.org/rnai/public/analysis-tools/sgrna-design) were used to identify and rank candidate CRISPR/Cas9 targets for predicted on- and off-target activities. For transient expression, sequences were ordered as overlapping 60-nt oligonucleotides, annealed and extended into a 100-bp duplex using Pfusion DNA polymerase, and cloned into an AflII-digested guide RNA expression vector (Addgene 41824) by Gibson assembly. Equal amounts of human codon-optimized Cas9 (Addgene 41815) and sgRNA vectors were transfected into HCT116 cells using FuGene 6 and into RPE cells using a Nucleofector 2b device (Lonza). For stable expression, target sequences were ordered as 24-nt oligonucleotides with asymmetric 5′ overhangs, phosphorylated with T4 polynucleotide kinase, then annealed and cloned into BsmBI-digested lentiGuide-puro (Addgene 52963) or pLenti-sgRNA (Addgene 71409) using T4 DNA ligase. Lentiviral transduction was performed as described above. Gene deletion was initiated by inducing a doxycycline-regulated Cas9 transgene present in the host cell line [14] or by infection with AdCas9 (ViraQuest).

Immunofluorescence microscopy and live-cell imaging

Antibodies used in this study are listed in the Key Resource Table. Cells were fixed and permeabilized in PEMFT (20 mM PIPES, pH 6.8, 10 mM EGTA, 1 mM $MgCl_2$, 4% paraformaldehyde, and 0.2% Triton X-100) for 13 min, blocked in 4% BSA, and stained with primary antibodies overnight. Species-specific secondary antibodies conjugated to Alexa Fluor 488, 564, or 647 were applied for 1 hr. Coverslips were mounted in ProLong Gold, imaged with a 100x oil objective on a DeltaVision Elite microscope (GE Life Sciences), and deconvolved in SoftWoRx using measured point spread functions. For timelapse experiments cells were grown in multiwell plates or 35 mm glass-bottom dishes (MatTek) and imaged on a Nikon Eclipse Ti microscope equipped with a stage-top incubator and CO_2 delivery system, 20x and 40x air objectives and 60x (1.4 NA) and 100x (1.45 NA) oil objectives, a Yokogawa CSU-X1 unit, and sCMOS (Andor Xyla 5.5) and EMCCD (Photometrics Evolve 512) cameras. Acquisition was performed with NIS Elements (v5.41). Epifluorescence and/or DIC images were acquired at 10-min intervals to measure mitotic arrest in response to spindle poisons, or at 2-min intervals to measure unperturbed mitotic timing. Confocal imaging of FLAP-Mad1 and H2B-mCherry was performed at 2- to 5-min intervals. Fluorescence intensities were quantified in ImageJ (v1.51) and analyzed in Prism 7.0 (GraphPad).

Correlative light-electron microscopy

Cells were fixed with 2.5% glutaraldehyde (Sigma) in PBS, pH 7.4-7.6 for 30 min, rinsed with PBS (3 × 5 min), and mounted in Rose chambers. Multimode (DIC and 3-color fluorescence) datasets were obtained on a Nikon TE2000 microscope equipped with a PlanApo 100x 1.45 NA objective lens at 53-nm XY pixels and 200-nm Z-steps. All LM images were deconvolved in SoftWoRx (v5.0) with lens-specific PSFs. Post-fixation, embedding, and sectioning were done as previously described [48]. Thin sections (70-80 nm) were imaged on a JEOL 1400 microscope operated at 80 kV using a side-mounted 4.0 megapixel XR401 sCMOS AMT camera (Advanced Microscopy Techniques Corp). Full series of images recorded at 10K magnification were used to reconstruct the volume of the cell, match orientation and superimpose this volume on the corresponding LM dataset. Higher-magnification images (40K) were then collected for individual kinetochores.

Cell lysis, immunoprecipitation, and western blotting

Cell extracts were prepared by resuspending pellets in ice-cold buffer B (140 mM NaCl, 30 mM HEPES, pH 7.8, 5% glycerol, 10 mM sodium pyrophosphate, 5 mM sodium azide, 10 mM NaF, 10 mM PMSF, 0.3 mM sodium orthovanadate, 20 mM b-glycerophosphate, 1 mM DTT, 0.2 mM microcystin, and 1x protease inhibitor cocktail (Sigma)) prior to nitrogen cavitation (1250 psi, 45 min; Parr Instruments) and centrifugation at 20,000 x g for 30 min. LAP-Rod was immunoprecipitated with GFP antibodies coupled to protein G-Dynabeads using bis(sulfosuccinimidyl)suberate (BS3). Zw10 was immunoprecipitated without BS3 crosslinking. Extracts and immunoprecipitates were separated by SDS-PAGE and transferred to PVDF or nitrocellulose membranes. Membranes were blocked and probed with primary antibodies and secondary antibody-HRP conjugates in 5% nonfat dry milk in TBST (Tris-buffered saline + 0.05% Tween-20) before detecting signals via enhanced chemiluminescence (Western Lightning Plus, PerkinElmer).

RT-PCR and sequencing

Total RNA was purified (RNeasy Mini kit, QIAGEN) and reverse-transcribed with random hexamers (SuperScript IV First-Strand Synthesis System, ThermoFisher). RT reactions were diluted 100-fold and amplified with *BUB1*-specific primers spanning exons 2-6 or exons 3-8. PCR products were cloned into pCR4 (TOPO-TA Cloning Kit, ThermoFisher) and sequenced with M13 reverse primer. Reads were trimmed and aligned in SeqMan Pro and annotated in SeqBuilder (DNASTAR LaserGene v14).

Please cite this article in press as: Rodriguez-Rodriguez et al., Distinct Roles of RZZ and Bub1-KNL1 in Mitotic Checkpoint Signaling and Kinetochore Expansion, Current Biology (2018), https://doi.org/10.1016/j.cub.2018.10.006

QUANTIFICATION AND STATISTICAL ANALYSIS

Quantitative data was compiled in Excel and analyzed using Prism 7.0. Details of each statistical analysis (number of cells (n), number of experiments (N), and measures of central tendency (mean or median)) are specified in the figure legends and Results. Unless stated otherwise, error bars indicate SEM $p \leq 0.05$ (with adjustment for multiple-hypothesis testing where applicable) was used as the significance threshold.